ACS Chemical Neuroscience

Research Article

Cite This: ACS Chem. Neurosci. 2018, 9, 2795−2806

pubs.acs.org/chemneuro

Metal Binding to Amyloid-β_{1-42}: A Ligand Field Molecular Dynamics Study

Shaun T. Mutter,[†] Matthew Turner,[†] Robert J. Deeth,[‡] and James A. Platts*[,†]

[†]School of Chemistry, Cardiff University, Park Place, Cardiff CF10 3AT, United Kingdom

[‡]Department of Chemistry, University of Warwick, Gibbet Hill, Coventry CV4 7AL, United Kingdom

Supporting Information

ABSTRACT: Ligand field molecular mechanics simulation has been used to model the interactions of copper(II) and platinum(II) with the amyloid-β_{1-42} peptide monomer. Molecular dynamics over several microseconds for both metalated systems are compared to analogous results for the free peptide. Significant differences in structural parameters are observed, both between Cu and Pt bound systems as well as between free and metal-bound peptide. Both metals stabilize the formation of helices in the peptide as well as reducing the content of β secondary structural elements compared to the unbound monomer. This is in agreement with experimental reports of metals reducing β-sheet structures, leading to formation of amorphous aggregates over amyloid fibrils. The shape and size of the peptide structures also undergo noteworthy change, with the free peptide exhibiting globular-like structure, platinum(II) system adopting extended structures, and copper(II) system resulting in a mixture of conformations similar to both of these. Salt bridge networks exhibit major differences: the Asp23-Lys28 salt bridge, known to be important in fibril formation, has a differing distance profile within all three systems studied. Salt bridges in the metal binding region of the peptide are strongly altered; in particular, the Arg5-Asp7 salt bridge, which has an occurrence of 71% in the free peptide, is reduced to zero in the presence of both metals.

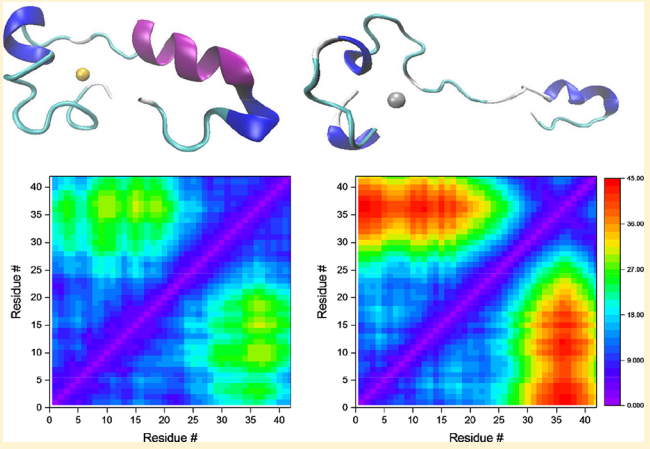

KEYWORDS: *Amyloid-β peptide, copper, platinum, Alzheimer's disease, ligand field molecular mechanics, ligand field molecular dynamics*

INTRODUCTION

Alzheimer's disease (AD) is a neurodegenerative condition, currently affecting more than 30 million people worldwide,[1,2] for which there is no cure. Common symptoms of AD include short-term memory loss, mild cognitive impairment, confusion and aggression. Over time, cognitive function degrades and control of bodily functions is lost, eventually leading to death. As a result, AD is the fourth most common cause of death in Western countries.[3]

The causes and development of the condition are not well understood, but AD is associated with damage to specific brain regions, the hippocampus and cerebral cortex,[4] involved in memory and cognition. AD brains exhibit abnormal structures, particularly deposits of neurofibrillary tangles and plaques,[5,6] formation of which is generally accepted to be the major pathological identifier of AD.[7] Amyloid-β (Aβ) peptide was first recognized as the main component of the deposited plaques in 1985[8] and has become the focus of much AD research in the decades since. In addition, brains show oxidative stress caused by reactive oxygen species (ROS)[9,10] and increased concentrations of metal ions, such as copper,[11] zinc,[4,12] iron,[13] and calcium.[14]

The amyloid hypothesis suggests that the buildup of Aβ in the brain is the main cause of AD and that amyloids are the main neurotoxic substance in disease progression. Individual Aβ monomers aggregate, leading to plaque formation.[15−18] This hypothesis suggests that Aβ possesses innate toxicity and that plaque deposits indicate an overload of Aβ, leading to disease.[19,20] An imbalance of Aβ generation and clearance leads to gradual accumulation of plaques in the brain.[15−18] Thus, the formation of these plaques leads to a local inflammatory response and subsequently to neuronal cell death, leading to gradual cognitive decline.[7,21] The rest of the known disease process, including the formation of neurofibrillary tangles, would then occur from this imbalance of Aβ generation and clearance.[21,22]

Received: April 30, 2018
Accepted: June 13, 2018
Published: June 13, 2018

DOI: 10.1021/acschemneuro.8b00210
ACS Chem. Neurosci. 2018, 9, 2795−2806

The structure and chemistry of Aβ has been reviewed in detail previously:[4,23−26] in monomeric form, Aβ is an intrinsically disordered peptide, adopting a random coil structure in aqueous solution.[27−29] Secondary structure and toxicity depend strongly on chemical conditions: in water, Aβ is reported to contain between 5% and 20% helical content and 0−25% β-sheet content, though the peptide remained mostly "random coil" in nature, as seen in PDB models 2LFM,[27] 1AML,[28] 1BA4,[30] and others.[25] In general, the C-terminus of Aβ is considered to form an extended helix-type structure. It has been shown that soluble oligomeric forms of Aβ are more toxic than mature plaques;[16,18,20] these oligomeric forms of Aβ are now increasingly believed to be the key toxic species in AD.[31−34] This structural variation poses challenges for studying Aβ, as identifying relevant conformations of the monomer is critical to understanding the oligomerization and aggregation process.[21,24]

Metal ions are known to play an important role in AD: disease progression correlates with the breakdown of Cu/Zn/Fe homeostasis in the brain.[4,35−37] These metals play a key role in the formation and stability of amyloid aggregates, and in the subsequent toxicity of Aβ. Increased levels of Cu(II) and Zn(II) are found in plaque regions of diseased brain,[38,39] and plaques which do not contain metal ions have been found to be nontoxic.[40] In addition, the redox activity of Cu(II) and Fe(II) indicate a possible mechanism for damage to brain cells, via generation of ROS.[41,42] As a result, the role of the natural metal ions in AD is increasingly studied, and are reviewed extensively elsewhere.[4,12,13,25,26] Recently, a new hypothesis has been put forward, suggesting a physiological role for the Aβ monomer as a metal binding and transport vehicle that acts to protect the brain from oxidative stress that results from elevated levels of metal ions.[23]

A great deal of experimental work, supplemented by extensive simulation, has elucidated details of metal−Aβ coordination. The hydrophilic N-terminal region of Aβ contains high-affinity metal binding sites, particularly the histidine (His)-rich region at residues 1−16. Varied metal coordination sites, including N-terminal histidines (His6, His13, and His14) and several oxygen ligands, such as alanine (Ala2), aspartic acid (Asp7), glutamic acid (Glu3, Glu11), and tyrosine (Tyr10) residues[43−46] have been proposed.

Copper(II) binds to Aβ through three N-donors and one O-donor (3N1O), with the specific choice of ligands being pH dependent: the predominant coordination modes are shown in Figure 1. These different binding modes, or components, have been experimentally resolved using continuous wave EPR spectroscopy on smaller fragments of Aβ.[43,47] Component I, which binds through Asp1, His6, and His13/14 is present at lower pH, approximately 6.5, whereas Component II binds through Ala2, His6, His13, and His14, and is the predominant form at higher pHs, approximately 7.4.

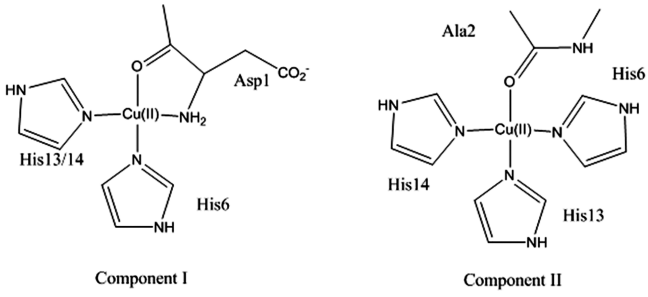

Figure 1. Copper(II) binding modes to the N-terminus of Aβ.

One possible route to AD-therapeutics involves disrupting the coordination of the native metal ions using compounds that selectively occupy the transition metal binding sites, hindering aggregation. This approach was pioneered by Barnham et al.,[48] who showed that Pt(II)(phenanthroline)Cl_2 complexes form adducts with Aβ bound through imidazole side chains of His6, and either His13 or His14. These complexes inhibit Aβ fibril formation and generate amorphous Aβ aggregates rather than fibrils. Pt(II)(phen) complexes also suppress hydrogen peroxide production by Cu(II)-Aβ_{42}, and Aβ toxicity in mouse neuronal cell cultures. Importantly, these complexes are not toxic at the concentrations required to produce this restorative effect. Work by Ma and co-workers showed that Pt(II)-Aβ binding at $[N_\varepsilon^{H6},N_\varepsilon^{H14}]$ predominates, while no coordination to His13 was detected.[49,50] In addition, Streltsov et al. used a combination of EXAFS and DFT to probe the local binding environment at Pt(II) and derive structural models for the interaction of Pt(II)(phen) complexes with Aβ_{16} and Aβ_{42}.[51]

DFT and ab initio methods have been used to investigate copper-Aβ interactions, but their computational expense typically requires the use of model systems such as Cu−Aβ_{1-16} or smaller.[52,53] In addition, hybrid quantum mechanics/molecular mechanics (QM/MM) was applied to Cu−Aβ_{1-16} to model energetics and redox potentials of different Cu-binding modes.[54,55] QM/MM combined with homology modeling was carried out by Ali-Torres et al.[54] to probe the Cu(II)−Aβ_{1-16} coordination sphere. The 3N1O model was considered with His6, His13 and His14 as nitrogen ligands, including δ and ε binding modes, with a range of potential residues for the oxygen ligand. A comparison of implicitly solvated free energy calculations revealed the most stable complex to contain the backbone carbonyl oxygen of the Ala2 residue (component II). This result was also in agreement with the experimental EPR results of Barnham and co-workers.[44] These calculations confirmed the preferential histidine binding modes to be $[O_c^{A2},N_\varepsilon^{H6},N_\delta^{H13},N_\varepsilon^{H14}]$.

Classical molecular dynamics simulations have also been used to study Cu−Aβ complexes. Raffa and Rauk[56] used DFT optimizations of model structures to benchmark Cu(II) parameters, which were used to study interaction with Aβ_{1-42} monomers and the effect of metal binding on secondary structure. Cu(II) was bound via water, His13, His14 and backbone N/O ligands; equilibration was observed after 350 ns, after which peptide structure was found to be dependent on the metal coordination mode. Huy et al.[57] used microsecond molecular dynamics simulations to model the structure and dynamics of Cu−Aβ_{1-42} monomer and dimer. Cu(II) was coordinated to His6, His13 (or His14), and Asp1 with distorted planar geometry. Cu(II) parameters were obtained from small model systems via UB3LYP calculations in implicit solvent. Pseudoequilibration of the metal-peptide complex was reached after several hundred nanoseconds of simulation; this revealed significant changes in the peptide salt-bridge and hydrogen-bond network upon Cu(II) coordination, as well as changes in peptide secondary structure and radius of gyration.

Ligand field molecular mechanics (LFMM)[58−60] is a powerful tool for the study of these transition metal-biomolecule interactions, able to provide "the flexibility and generality of quantum mechanics with the speed of molecular

DOI: 10.1021/acschemneuro.8b00210
ACS Chem. Neurosci. 2018, 9, 2795−2806

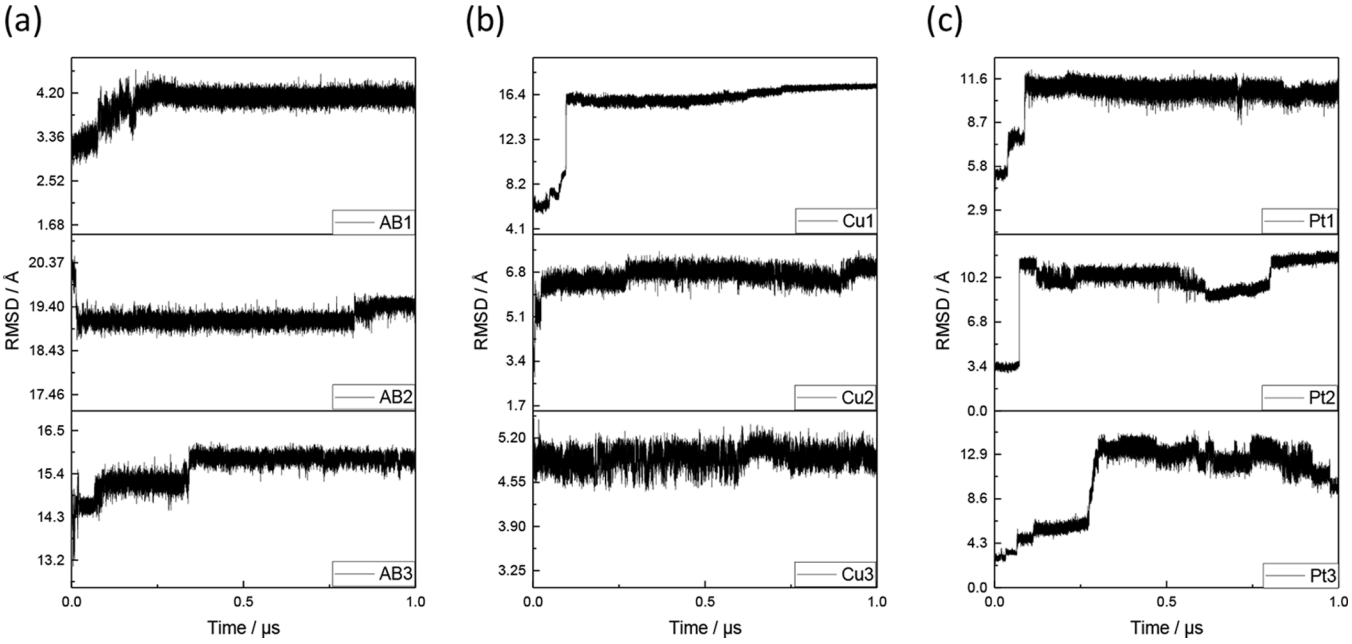

Figure 2. RMSD (Å) against initial structure of each trajectory, against time (μs) for AB (a), Cu (b), and Pt (c).

mechanics".[61] Here the Ligand Field Stabilization Energy (LFSE) in these complexes is captured in a small number of transferable parameters. LFMM has seen success in modeling a range of Jahn−Teller active Cu(II) systems,[62] spin states of Ni and Fe complexes[63] and Pt(II)-biomolecule studies.[64,65] Recently, we have shown the suitability of LFMM for description of binding of Cu(II)[66] and Pt(II) with fragments of Aβ.[67−69]

In this work, we extend this LFMM approach to examine the dynamical behavior of Cu(II)− and Pt(II)(phen)−Aβ complexes using molecular dynamics simulations and LFMM description of metal coordination coupled with conventional molecular mechanics (MM) for the peptide.

RESULTS AND DISCUSSION

Conformational databases for the Aβ_{42}, Cu(II)−Aβ_{42}, and Pt(II)−Aβ_{42} systems (denoted AB, Cu and Pt, respectively) generated from LowMode molecular dynamics simulations were used to select starting structures for use in the ligand field molecular dynamics (LFMD) simulations. Three distinct low energy conformations (i.e., with mutual root-mean-square deviation (RMSD) greater than 1.5 Å) were chosen for each system, to enable better sampling of conformational phase space. LFMD simulations of 1 μs were carried out for each starting point, denoted 1−3, preceded by AB, Cu, and Pt, for Aβ_{42}, Cu(II)-Aβ_{42}, and Pt(II)-Aβ_{42}, respectively.

Aβ peptides are intrinsically disordered, such that full equilibration is beyond current computational capabilities. Therefore, we have utilized the description of quasi-equilibration reported by Huy et al.,[57] who used RMSD fluctuations around a stable value after several hundred nanoseconds as their criteria to determine equilibration. Use of several trajectories with different starting points that have been quasi-equilibrated allows for greater analysis of phase space. Figure 2 shows RMSD for three microsecond trajectories of each of AB, Cu, and Pt. Quasi-equilibration times taken from these data were 0.30, 0.10, and 0.40 μs for AB1, AB2, and AB3; 0.20, 0.30, and 0.10 μs for Cu1, Cu2, and Cu3; and 0.25, 0.25, and 0.40 μs for Pt1, Pt2, and Pt3, respectively. These assignments are supported by radius of gyration (R_g) across the trajectories, which are reported in the Supporting Information.

Trajectories beyond equilibration were used for further analysis to compare the structural and dynamical differences between the free Aβ and peptides coordinated with Cu(II) and Pt(II). The data obtained for each trajectory has been averaged, over representative number of frames, for effective comparison between the three systems of interest. Average RMSD, along with standard deviation, maximum, and minimum values, is reported in Table 1. Low standard deviation values are observed, particularly for AB and Cu, further supporting our assignment of equilibration times. Pt3 is the only trajectory resulting in a standard deviation greater than 1 Å, although this is within the range to be considered quasi-equilibrated.[57]

Table 1. RMSD (Å) of AB, Cu, and Pt

	avg RMSD	SD	max	min
AB1	4.12	0.08	4.56	3.75
AB2	19.15	0.16	19.71	18.71
AB3	15.79	0.11	16.22	15.20
Cu1	16.39	0.58	17.56	14.98
Cu2	6.77	0.23	7.93	5.78
Cu3	4.92	0.13	5.40	4.42
Pt1	10.86	0.34	12.18	8.55
Pt2	1.033	0.94	12.30	8.24
Pt3	12.55	1.09	15.23	8.70

Radius of gyration, R_g, quantifies the size and compactness of a peptide: data reported in Table 2 shows how metal coordination affects the size of Aβ. On average, the free Aβ peptide is the most compact of the three systems, with a mean value of 9.62 Å and a standard deviation across three trajectories of 0.66 Å. This average value compares reasonably well with values obtained from ion mobility cross sections measurements of 10 to 15 Å.[70] Pt trajectories are also quite

DOI: 10.1021/acschemneuro.8b00210
ACS Chem. Neurosci. 2018, 9, 2795−2806

Table 2. Radius of Gyration (Å) of AB, Cu, and Pt

	avg R_g	SD	max	min
AB1	9.07	0.04	9.27	8.90
AB2	9.43	0.14	9.83	8.91
AB3	10.73	0.09	11.19	10.15
all AB	**9.62**	**0.66**	**11.19**	**8.90**
Cu1	21.72	0.57	22.83	20.32
Cu2	11.18	0.21	12.04	10.28
Cu3	9.13	0.07	9.47	8.82
all Cu	**13.78**	**5.53**	**22.83**	**8.82**
Pt1	16.28	0.27	17.29	14.65
Pt2	15.51	1.05	17.82	13.35
Pt3	17.97	0.95	20.17	14.36
all Pt	**16.49**	**1.29**	**20.17**	**13.35**

consistent, giving rise to more extended geometries and an average R_g of 16.49 Å. The phenanthroline ligand also has some contribution to this higher value, with a R_g of 2.29 Å, when coordinated to just platinum. While, on average, the Pt exhibits the least compact structure, the individual Cu trajectories show that it occupies two distinct structural conformations, with R_g values of 9.13/11.18, and 21.72 Å, meaning that it occupies states similar to both the free peptide and the platinated system.

Figure 3 reports the percentage secondary structure of the AB, Cu, and Pt trajectories. One letter codes C, I, G, H, B, E, and T correspond to the structure elements coil, π-helix, 3_{10} helix, α-helix, β-bridge, β-sheet, and turn, respectively. As expected for intrinsically disordered peptides, there is large percentage of coil and turn structure for all three systems. AB also exhibits 3_{10} helical structures at residues Asp7-Gly9 and Ser26-Ile31, in agreement with an experimentally resolved structure of the related Aβ_{40} peptide in aqueous solution.[27] In addition, several residues occupy β-bridge conformations for significant periods of simulation time and there is a small occurrence of α-helix in the central hydrophobic region (residues Leu17-Ala21) of the peptide.

Copper coordination induces significant helical character, both α- and 3_{10}- in nature, in the region of residues Asp23-Leu34 and toward the C-terminus of the peptide, as shown by a snapshot shown in Figure 4, as well as the prevalent turn and coil structure. There is also helical character at residues Glu11-Phe20, which centers on two of the coordinating residues (His13 and His14), including a small amount of π-helix, which is not present in either the free AB or Pt. Cu also exhibits a significantly smaller population of β-bridge conformations, with only residues Ile32 and Val39 showing a minimal amount of this.

As for free AB and Cu, there is a predominant occurrence of turn and coil structure for the Pt. There is also 3_{10} helical character at several regions of this coordinated peptide, including residues Glu3-Arg5, Val12-Lys16, and Ala30-Val36, as shown by a snapshot in Figure 4. There is a mix of α- and 3_{10}-helix in Val18-Gly25, albeit with a lower occurrence than the rest of the helical regions in this system. The C-terminus also exhibits some β-bridge structures, albeit with lower occurrence than AB, but greater than Cu.

The tertiary structure of each system has been mapped via distances between Cα in each residue with all other Cα, plotted as a heat map in Figure 5. The contact maps between the residues is consistent with R_g values reported above. The longer distances (shown as red) observed for Pt, especially in the region of [(Asp1-Phe20), (Ala30-Val40)], show that on average there is very little contact between the N- and C-termini of the peptide, with distances between α-carbons between 33 and 41 Å. The termini of the peptide, i.e. residues 1 to 23 and 29 to 42, remain fairly compact. Beyond the central hydrophobic cluster, in the C-terminal direction, this system exhibits an extended conformation, as shown by the sharp increase in distance.

Cu exhibits a similar contact map, and therefore overall structure, to Pt but with significantly smaller distances between the termini, as shown by larger green areas, corresponding to distances of 20−29 Å. In contrast, AB shows a rather compact structure, with the largest distances between α-carbons in the region [(Tyr10-Phe20),(Met35-Val40)] with a maximum distance of approximately 21 Å. The smaller distances between the residues at N- and C- termini also show that this system lacks any of the extended structure observed for Pt.

The numbers of hydrogen bonds for the three systems have also been calculated and are reported in Table 3. On average, the presence of coordinated metals reduces the number of hydrogen bonds, as might be expected from the differences in structure determined from results above. High standard deviation values are observed throughout, alongside a large range between minimum and maximum values for all systems, suggesting that the hydrogen bonds are highly transient.

Figure 6 shows the root-mean-square fluctuation (RMSF) per residue of the three systems of interest, showing the average mobility of the peptide backbone atoms across trajectories. This data shows that AB generally has the lowest RMSF values across the whole simulation time. Cu has comparable values to AB, in general having slightly larger RMSF values. Exceptions to this pattern are found for coordinated residues (2, 6, 13, and 14), as well as the central hydrophobic cluster (17−21). In contrast, Pt exhibits much larger RMSF values across the whole sequence: this is even true for residues that are bound to Pt (6 and 14). The residues at the C-termini of the copper and platinum systems also show much greater RMSF values than those at the N-termini, whereas the free peptide has consistently low values across all residues. Analysis of each individual trajectory can be found in the Supporting Information: AB shows great consistency across trajectories, whereas there is greater deviation between trajectories for Cu and Pt.

At physiological pH, there are three positively charged and six negatively charged residues in Aβ_{42}, potentially leading to a maximum of 18 salt bridges. The presence or absence of each possible salt bridge have been calculated across all equilibrated trajectory data. It should be noted that, due to the definition of such contacts used in VMD, it is possible for a single residue to form multiple salt bridge type interactions at the same time, such that cumulative percentages for that residue can exceed 100%. Figure 7 shows averaged salt bridge contact maps for AB, Cu, and Pt.

In AB, 13 of the possible salt bridges are observed, although many are present for less than 50% of total simulation time. Lys16-Glu11, Lys16-Glu22, and Arg5-Asp7 are present in approximately 90% of frames, indicating that these residues remain in close proximity throughout. In comparison, copper coordination leads to fewer salt bridges, with only six occupied. Once again, there is a recurrent Lys16−Glu11 interaction, which is 100% present throughout the simulation. Arg5 forms salt bridges with Glu22 and Asp23, contacts that are not observed for the free peptide. However, this basic residue loses

DOI: 10.1021/acschemneuro.8b00210
ACS Chem. Neurosci. 2018, 9, 2795−2806

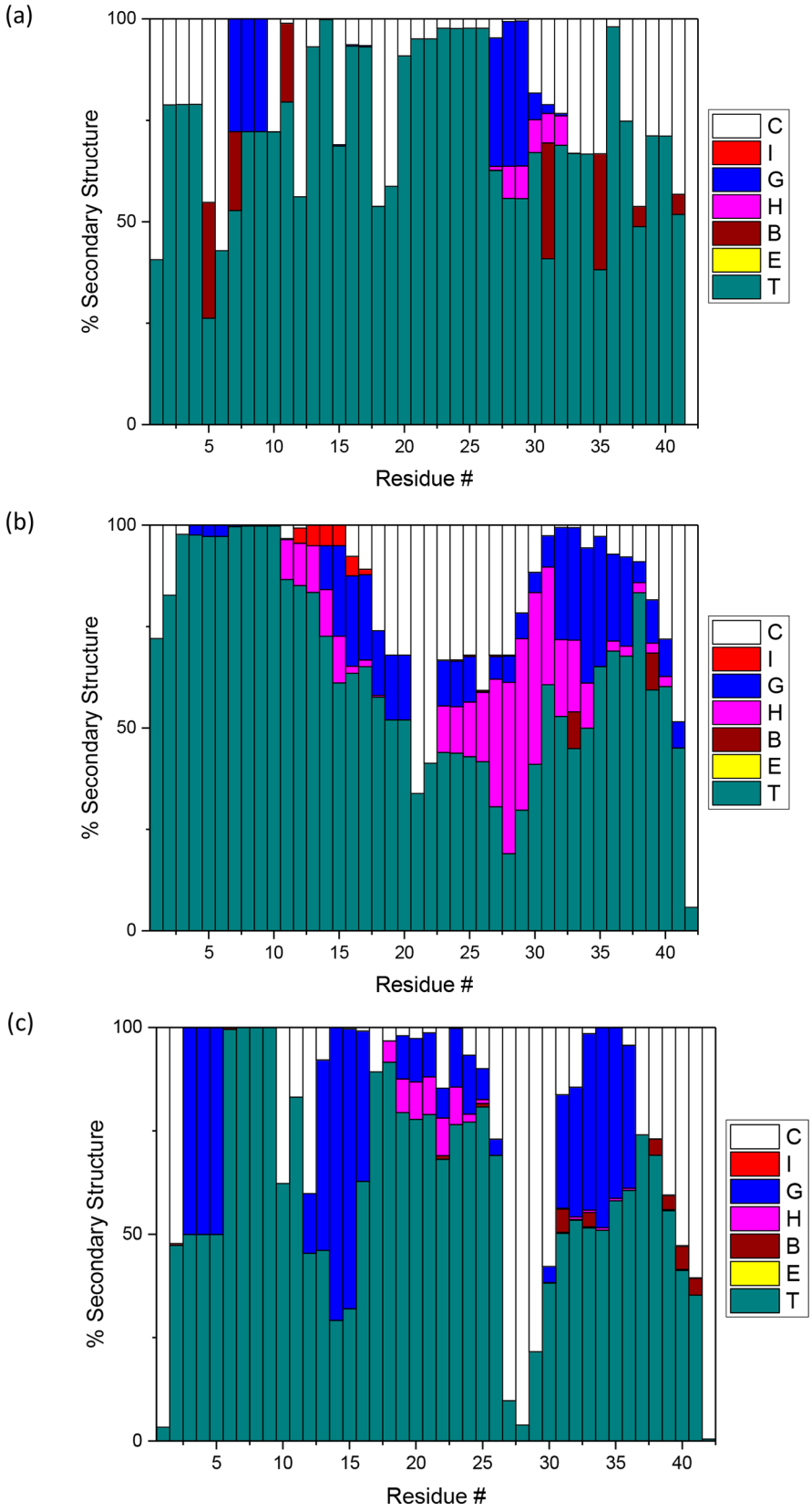

Figure 3. Percentage secondary structure of AB (a), Cu (b), and Pt (c). C, I, G, H, B, E, and T correspond to the structure elements coil, π-helix, 3_{10} helix, α-helix, β-bridge, β-sheet, and turn, respectively.

all contact with Glu3, Asp7, and Glu11 when Cu(II) binds, showing that metal coordination significantly disrupts the salt bridge network at the N-terminus. Lys28 also shows fewer interactions for Cu, only forming bridges with Asp1 and Asp23.

DOI: 10.1021/acschemneuro.8b00210
ACS Chem. Neurosci. 2018, 9, 2795−2806

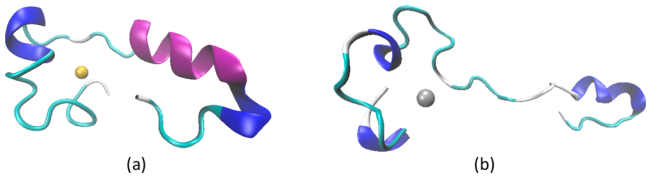

Figure 4. Selected snapshots of Aβ_{42} systems represented by ribbon structures: (a) Cu and (b) Pt. White, green, blue, and pink sections correspond to coil, turn, 3_{10}-helix, and α-helix, respectively. Copper and platinum are shown as yellow and silver spheres, respectively. Phen ligand is omitted for clarity.

Platinum binding also leads to significant differences from both free and copper coordinated systems. Once again, coordination leads to loss of the Arg5-Asp7 salt bridge, suggesting that coordination to His6 prevents formation of this interaction. The Glu11-Lys16 contact, while still present, is much less populated: again, metal coordination between these residues apparently affects the ability of the peptide to form such a contact. Unlike Cu, Pt(II) complexation allows the Lys16-Glu22 interaction to persist, as in the free peptide. The platinated system also lacks the Lys28-Asp1 salt bridge, which is present approximately 25% of the time in the other two systems.

The extensive data gathered for all three systems allows for further analysis of how the two different metals affect the structure and dynamics of the peptide and allows for comparison against the unbound system. RMSD and R_g data show large variance in values between trajectories after equilibration has been reached. This is particularly evident for Cu, where Cu1 equilibrates to R_g of 22 Å, while Cu2 and Cu3 equilibrate to 11 and 9 Å, respectively. This indicates a significant change in the compactness of the peptide between trajectories. Further examination shows that Cu1 undergoes a conformational change at approximately 0.1 μs, away from the globular structure observed throughout trajectories Cu2 and Cu3, to a more extended structure. Snapshots from the end of each trajectory are reported in Figure 8a. The conformation adopted by Cu1 is similar to that observed for all three Pt systems, which have an average R_g value of 16.49 Å, (snapshots shown in Figure 8b). Structures from the Cu2 and Cu3 trajectories show a greater similarity to those of the free peptide, which have an average R_g value of 9.62 Å (Figure 8c).

The conformational change during Cu1 can also be easily observed within the changing secondary structure over the trajectory. The N- and C-termini are largely unchanged, but significant differences are observed after 0.1 μs for the central portion of the sequence, Leu17 to Ala30, which is initially a mix of turn and helix but becomes strongly coil like after the conformational change. The hydrogen bonding network in Cu1 includes contact between Glu22 and Ser28 that is prevalent during the first 0.1 μs, whereas after this point there are no occurrences of this H-bond. Conversely, several H-bonds are common after 0.1 μs, particularly Arg5-Asp23, Glu3-Tyr10, and Glu11-Gln15, with occupancies of 86%, 76%, and 68%, respectively. These residues are not involved in any significant H-bonding in the Cu2 and Cu3 trajectories.

Table 3. Hydrogen Bond Count for AB, Cu, and Pt

	avg H-bond #	SD	max	min
Aβ1	13.98	2.80	26	2
Aβ2	10.52	2.40	22	2
Aβ3	13.25	2.74	24	3
all Aβ	**12.61**	**3.05**	**26**	**2**
Cu1	9.34	2.49	20	1
Cu2	10.36	2.53	21	1
Cu3	10.12	2.74	25	1
all Cu	**9.90**	**2.63**	**25**	**1**
Pt1	11.64	2.49	23	2
Pt2	11.50	2.43	22	2
Pt3	8.97	2.36	19	0
all Pt	**10.82**	**2.70**	**23**	**0**

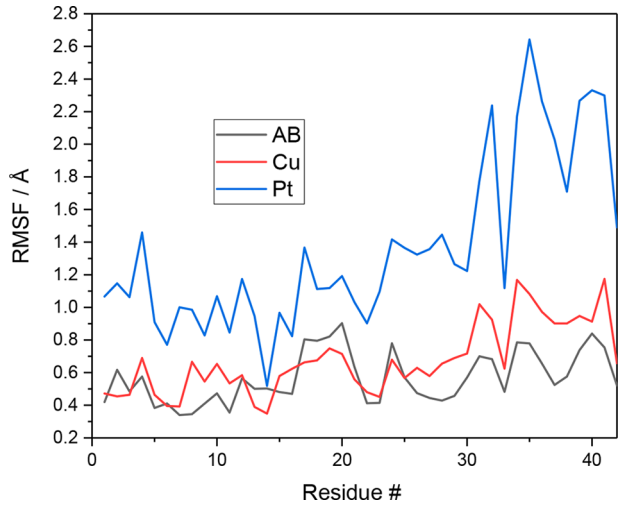

Figure 6. Root mean square fluctuations (RMSF) of AB, Cu, and Pt. Corresponding numerical data can be found in the Supporting Information.

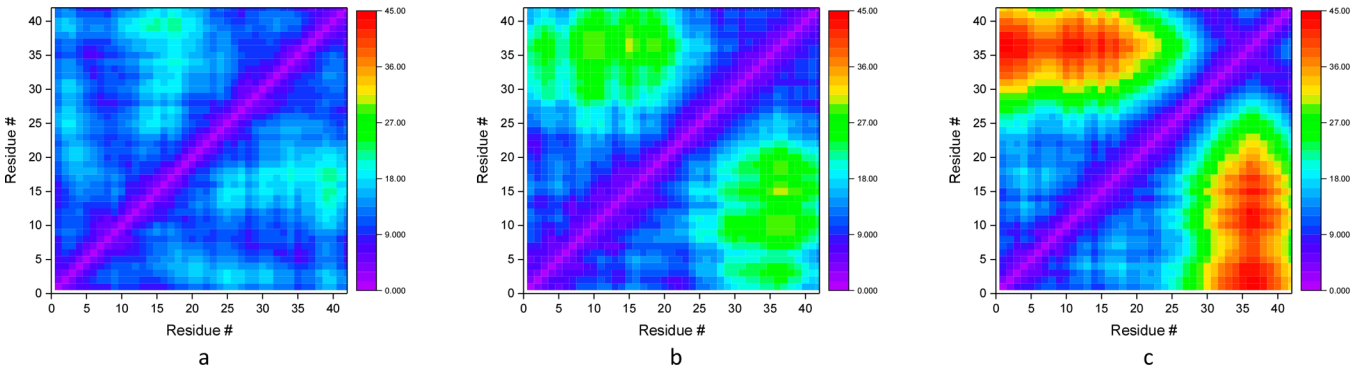

Figure 5. Residue contact maps, based on α carbon distances (Å), of AB (a), Cu (b), and Pt (c).

DOI: 10.1021/acschemneuro.8b00210
ACS Chem. Neurosci. 2018, 9, 2795−2806

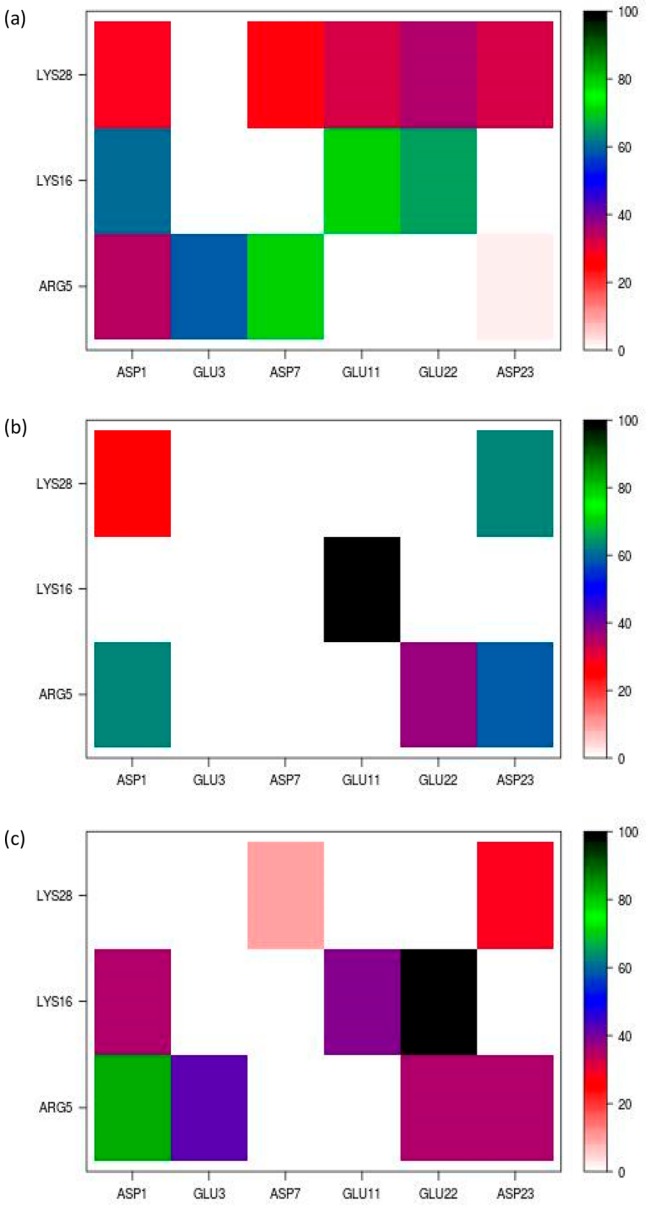

Figure 7. Salt bridge contact maps, percentage occurrence, for AB (a), Cu (b), and Pt (c). Corresponding numerical data may be found in the Supporting Information.

Hydrogen bonding between Glu22 and Ser28, seems to have some significance in the overall structure of Cu, as in trajectories Cu2 and Cu3 this interaction has an occupancy of 62% and 43%, respectively.

Simulations on the free Aβ_{42} monomer in aqueous conditions, with varying force fields and implementations, have shown that coil dominates the ensemble, along with 5−20% helical character and 0−15% β character.[25] This is in good agreement with results presented here (Figure 3) where we find helical and β-like populations of approximately 5% and 3%, respectively. However, turn-like structure dominates over random coil here with populations of 69% and 23%, respectively. This aligns with the work of Yang and Teplow[71] who used extensive replica exchange MD simulations and found that the expected random coil ensemble was separated by regions of highly populated turn structure between residues.

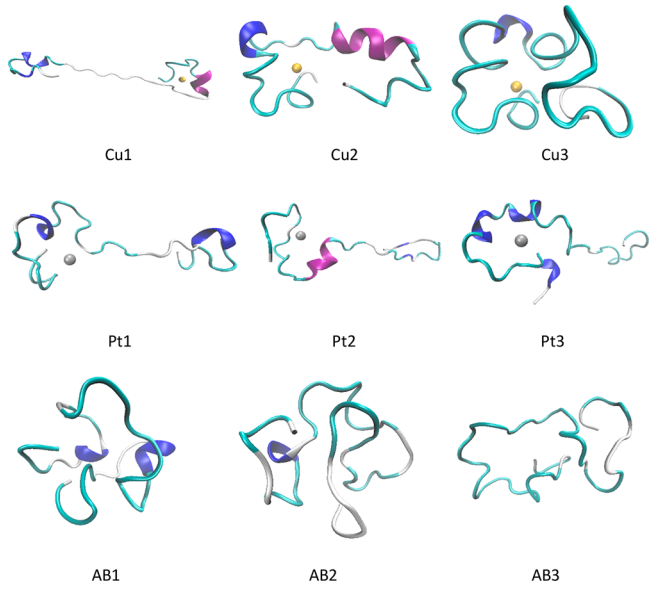

Figure 8. Final frame of the trajectories for (a) Cu, (b) Pt, and (c) AB.

They reported that, for nonterminal residues, that turnlike structure contributed 30−80% of the overall peptide structure.

Within Cu, there is strong helical character, both α- and 3_{10}-helix, in the central hydrophobic cluster and from Asp23 toward the C-terminus of the peptide, as shown by a snapshot in Figure 8. There is also helical character at residues Glu11-Phe20, which centers on two of the coordinating residues (His13 and His14), including a small amount of π-helix, which is not present in either AB or Pt. The copper system also exhibits a significantly smaller population of β-bridge conformations, with only residues Ile32 and Val39 showing a minimal amount of this. This is in agreement with available experimental data, in that copper enables formation of amorphous aggregates over amyloid fibrils due to decrease in β character.[40] Our data is also in broad agreement with previous simulation studies: Huy and co-workers[57] found a drop in β-structure from approximately 10% down to 0.6% within Aβ42 upon copper coordination, which is similar to the observed drop here of 3% to 0.4%. However, our longer simulations find an increase in helical character on copper coordination, especially around the central hydrophobic cluster and toward the C-terminus, compared to a slight reduction in Huy et al.'s work.

As would be expected, metal coordination has a pronounced effect on the secondary structure of the peptide in the metal binding region. Both Cu(II) and Pt(II) reduce the content of β-bridge to zero and alter the residues that form helices. The 3_{10}-helix observed for residues Asp7-Gly9 is not present in either metalated system, where it is entirely turn structure. This is likely a result of metal binding to the neighboring His6 residue, breaking this structure element. There is also a difference between the secondary structure of the metals' coordination spheres: platinum results in a 3_{10}-helix at Glu3-Arg5, compared with less than 3% of this structure in Cu. This region is flanked by two residues that both coordinate to copper, where the platinum only has coordination to His6, meaning that for copper there is less flexibility to form different structural elements. A similar observation can be made for the His13-His14 region, whereby copper binds to both and

DOI: 10.1021/acschemneuro.8b00210
ACS Chem. Neurosci. 2018, 9, 2795−2806

platinum only binds to the latter. For the copper binding residues, some helical character is observed (ca. 12%) but the remainder is turn dominated. Platinum once again exhibits a mix of turn and 3_{10}-helix at the His14 residue, and none of the other helical structure elements seen for copper. Beyond the copper having two additional binding sites, the platinum's relatively bulky phen ligand is the major difference which, as shown by RMSF and residue contact maps, gives a less compact N-terminus and allows for greater flexibility. These differences are key in the different peptide structural behavior observed.

One of the more pronounced differences between the free peptide and the metalated LFMD simulations is the content of helical secondary structure elements. AB overall has an occurrence of less than 5%, whereas Cu and Pt have helical content of >19% and >16%, respectively. From these results, it is clear that both metals stabilize helices within Aβ, which has shown to potentially destabilize fibril formation and instead lead to amorphous aggregates.[71] This also has other possible implications in the progression of AD, where Kepp[23] has postulated that a loss of functional Aβ monomer is the root cause of disease. Therefore, the stabilization of helices by copper, along with maintaining the monomer's biological functions, suggests that copper does not exclusively contribute to fibril formation. Platinum also stabilizes helices, but competition with copper at the metal-binding region may impair monomer function.

RMSF data presented in Figure 6 shows that metal coordination increases the mobility of the Aβ peptide. This is particularly evident for Pt, which has the greatest RMSF values across the entire peptide, with values peaking for residues in the C terminus. A similar pattern is observed for Cu, with residues past Leu34 having the highest RMSF values for this system. The conformations exhibited by Pt and the Cu1 trajectory provide some explanation of this, in that the spatial separation of the peptide termini allows the C-terminus to be more mobile. In comparison, the N-termini of the copper and platinum systems are constrained by the metal coordination, as shown by the lower RMSF values for the coordinating residues. The more compact nature of the free peptide systems leads to the lower RMSF values as well as the even distribution of mobility across the entire peptide.

Comparing RMSF of the AB and Cu shows that coordination results in greater mobility of the peptide backbone with exceptions for the coordinating residues, due to the restriction of the metal binding, and the central hydrophobic cluster. Val24 also exhibits a marginally higher RMSF for free peptide. The central hydrophobic cluster is known to be important in fibril formation, as contacts between this region and the C-terminus have been found to destabilize fibrils and more likely result in amorphous aggregates.[71] The observation that Cu(II)-coordination reduces mobility of this region might therefore suggest a role for metals in affecting oligomerization. The relatively bulky phenanthroline ligand on the platinum, along with only two coordinating residues, results in a less compact N-terminus compared to the copper systems, with four coordinating residues. This can be observed in the contact maps for residues in the N-termini in Figure 5. The less compact nature of the platinum coordination site allows for greater conformational flexibility resulting in the greater RMSF values seen for the platinated systems.

Figure 9 gives more detail on the effect of metals on the Asp23-Lys28 salt bridge, which is known to be important for aggregation into fibrils.[72] AB shows a sharp peak around 4.0 Å, and two broader peaks around 4.7 and 6.0 Å: no recorded frame has a distance greater than 7 Å, such that even in configurations not classified as containing this salt bridge the residues remain in general proximity of one another. Copper coordination increases the prevalence of close contacts, and reduces the peak distance to around 3.5 Å. However, 30% of configurations are also present where these residues are fully separated at more than 20 Å apart. Platinum coordination is broadly similar to Cu(II), with a sharp peak at shorter separation than in the free system, but also with 67% of configurations in which Asp23-Lys28 are more than 10 Å apart.

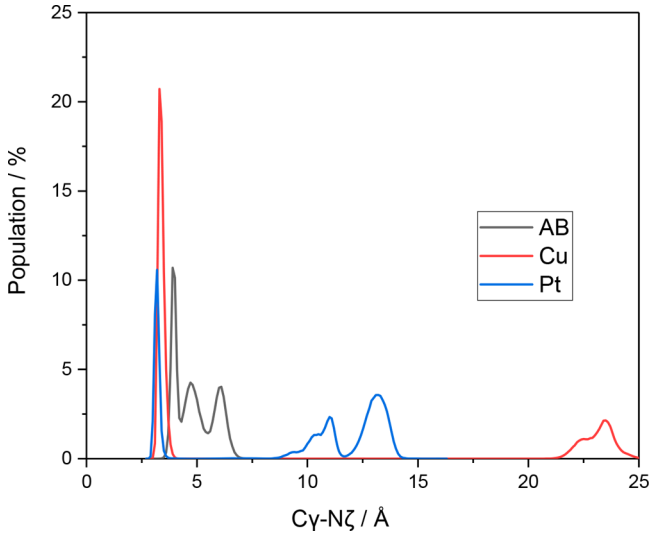

Figure 9. Asp23-Lys28 salt bridge distance distribution (Å) against percent of occurrence.

As shown in Figure 7 above there is a salt bridge between residues Asp5-Arg7 in the free peptide, with an occurrence of 71%, which is no longer present after coordination. Figure 10 shows the distance distribution of this salt bridge, for the three systems, in greater detail. AB shows a sharp peak at approximately 4 Å, with a smaller shoulder at 3.5 Å,

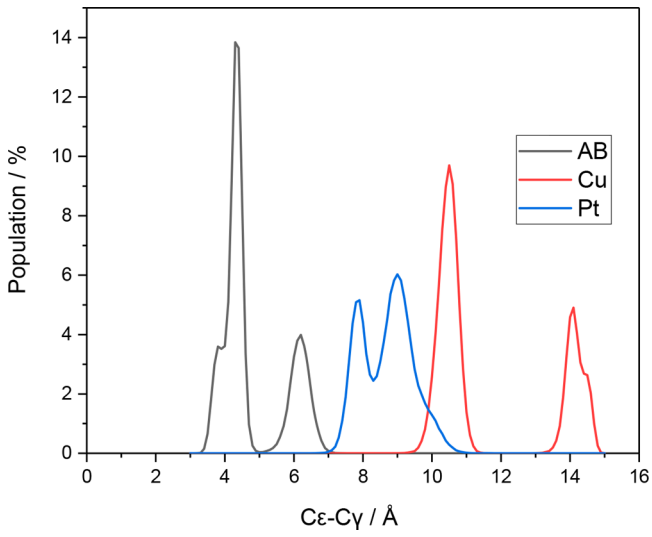

Figure 10. ARG5-ASP7 salt bridge distance distribution (Å) against % occurrence.

DOI: 10.1021/acschemneuro.8b00210
ACS Chem. Neurosci. 2018, 9, 2795−2806

corresponding to the presence of the salt bridge. The peak at 6.2 Å represents the 29% of the trajectories where this salt bridge does not occur, but no frames are found where this distance is greater than 7 Å. In contrast, both Cu and Pt trajectories lack this salt bridge in all frames, with no distance less than 9 and 7 Å, respectively. Figure 11 reports snapshots of these systems, showing how metal coordination at His6 leads to the side chains pointing away from each other, with no such effect in the free peptide. It seems clear, therefore, that metal coordination to HIS6 must lead to loss of this salt bridge and hence disruption of the structure of the N-terminus. This may then have an effect on the structure and aggregation of Aβ, although these monomer simulations cannot yield any information on this. These snapshots also suggest a role for the phenanthroline ligand, which leads to a less compact, more flexible N-terminus, which may explain the closer contact of Asp5 and Arg7 compared to Cu.

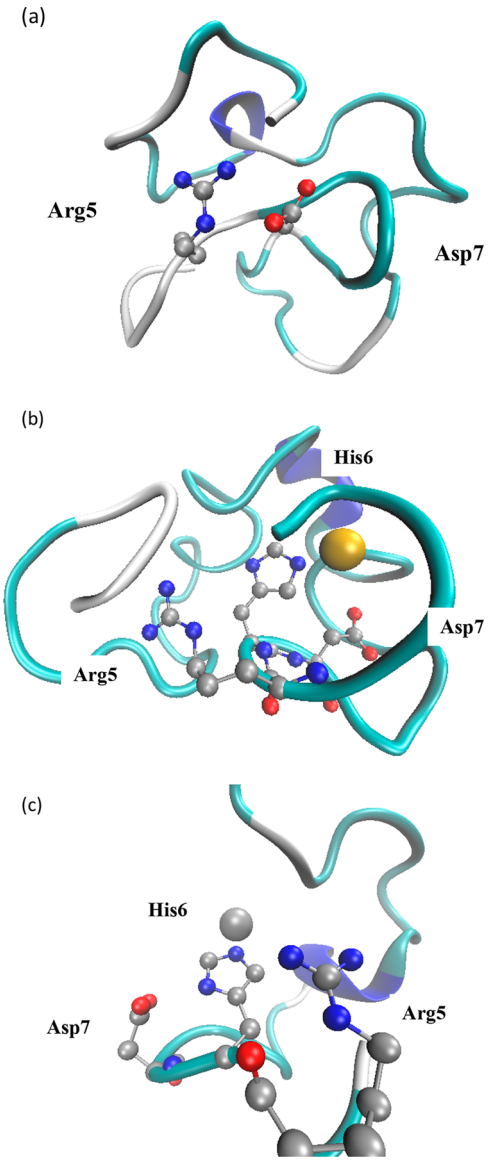

Figure 11. ARG5-ASP7 taken from (a) last frame of AB2, (b) last frame of Cu3, and (c) last frame of Pt1. Phen ligand omitted for clarity.

CONCLUSIONS

Analysis of the data extracted from the LFMD simulations show that it is clear that coordination by copper and platinum has a significant and different effect on the structure and dynamics of the Aβ peptide. Platinum results in extended structures, with large displacement between the termini and greater flexibility of most residues, especially those toward the C-terminus. Copper binding results in a mix of conformations, adopting structures that are "platinum-like" as well as others that are close to those for the free peptide. Secondary structure analysis shows that both metals stabilize helices, with similar overall quantities of this structural element. Platinum has more 3_{10}-helix whereas copper has approximately equal amounts of 3_{10}- and α-helix. The peptide regions within which these occur also differs, with copper having the majority of helices in the central hydrophobic cluster and toward the C-terminus, while platinum induces greatest helical content near the N-terminus.

Conformational differences are reflected in the differing salt bridge networks. Asp23-Lys28, which has implications in aggregation, is significantly altered under metal coordination. In the free peptide this salt bridge is present in 33% of the time, but in all frames the individual residues are in close contact. Cu and Pt, despite having occurrences of 63% and 29%, respectively, show different patterns: the salt bridges that do occur have smaller distances between charged moieties, but the remaining frames have such a large separation that it would not be possible for the salt bridge to reoccur without major conformational rearrangement. The Arg5-Asp7 salt bridge also shows significant differences when metal binding occurs, dropping from 71% to 0% for both Cu and Pt. The binding of the metal to the residue between this salt bridge directly causes this difference as the charged side-chains are no longer able to orient to form this interaction.

The differing dynamical and structural observations for Cu and Pt appear to arise from the nature of the coordination sphere. Despite the metals sharing two coordinating residues, the significance of the copper also binding to one neighboring residue and to the residue adjacent to the N-terminus, along with the effects of the bulky phenanthroline ligand, cannot be understated. Copper binding at residues Ala2, His6, His13, and His14 results in a more restrictive and compact coordination sphere. In comparison, platinum binding at His6 and His14, combined with the additional ligand, allows for a greater backbone mobility and structural flexibility for this region.

Metal binding to Aβ plays a pivotal role in the progression and onset of AD, but at present that exact role is still largely disputed. Understanding the differences that occur at the coordination site and the peptide beyond, and how the conformation and dynamics can be significantly altered will lead to a greater knowledge of this devastating disease.

METHODS

Ligand field molecular dynamics (LFMD) simulations were carried out using DL_POLY_LF,[65] which incorporates LFMM within DL_POLY2.0.[73] LFMM parameters for Cu(II) and Pt(II) have been tested and reported previously,[66,69] while AMBER PARM94 parameters have been used for all other atoms.[74] Aβ_{1-42} was constructed in extended conformation within MOE,[75] with the appropriate residue protonation states for physiological pH. Cu(II) was coordinated in a $[O_c^{A2},N_\varepsilon^{H6},N_\delta^{H13},N_\varepsilon^{H14}]$ binding mode, while Pt(II)-phenanthroline was coordinated in a $[N_\varepsilon^{H6},N_\varepsilon^{H14}]$ binding mode. Partial charge assignment was carried out using MOE's dictionary lookup, then modification to the metal and coordination

DOI: 10.1021/acschemneuro.8b00210
ACS Chem. Neurosci. 2018, 9, 2795−2806

sphere charges was carried out as reported previously, with values reported in Tables S1 and S2.[66,69]

LowMode molecular dynamics simulations[76] were carried out within the DommiMOE[60] extension to MOE to generate diverse starting points for LFMD simulations.[67] DL_POLY input files were generated using DL_FIELD3.5[77] and DommiMOE, for the free $A\beta_{1-42}$ and the metal bound $A\beta_{1-42}$, respectively. All LFMD simulations were carried out within the NVT ensemble, with a 1 fs integration time step, for 1 μs. Nosé-Hoover thermostat, with relaxation constant of 0.5 ps, was used to control temperature at 310 K. Reaction field electrostatics were used throughout with a van der Waals cutoff of 10 Å and long-range electrostatic interaction cutoff of 21 Å. The SHAKE algorithm,[78] with a tolerance of 10^{-8} Å, was used to constrain all bonds to hydrogen. Atomic positions and velocities were recorded every 10 ps for subsequent analysis.

Analysis of all the LFMD trajectories was carried out using VMD 1.9.2.[79] RMSD and R_g were utilized for equilibration tests. The timeline extension was used to analyze secondary structure (using the STRIDE algorithm),[80] RMSF, hydrogen bonds, and salt bridges. Residue contact maps were recorded using the iTrajComp VMD plugin.[81] The presence of a hydrogen bond was determined by a donor−acceptor distance of less than 3 Å with an angle of less than 20°. Salt bridges were defined as any contact distance of less than 3.2 Å between oxygen and nitrogen atoms in charged residues.

■ ASSOCIATED CONTENT

Supporting Information

The Supporting Information is available free of charge on the ACS Publications website at DOI: 10.1021/acschemneuro.8b00210.

Partial charges for copper and platinum coordination spheres; radius of gyration plots of full microsecond trajectories; tabulated root-mean-square fluctuations for individual trajectories; tabulated salt bridge data (PDF)

■ AUTHOR INFORMATION

Corresponding Author

*E-mail: platts@cardiff.ac.uk. Phone: +44-2920-874950. Fax: +44-2920-874030.

ORCID

Robert J. Deeth: 0000-0001-7933-4406

James A. Platts: 0000-0002-1008-6595

Author Contributions

All authors designed experiments; S.T.M. and M.T. carried out simulations; S.T.M., M.T., and J.A.P. analyzed data; all authors wrote the manuscript.

Funding

This work was funded in part by the UK Engineering and Physical Sciences Research Council under grant ref EP/N016858/1.

Notes

The authors declare no competing financial interest.

Trajectory data can be obtained from DOI 10.5281/zenodo.1289166.

■ ACKNOWLEDGMENTS

Computing facilities were provided through Cardiff University's Advanced Research Computing @ Cardiff (ARCCA) facility.

■ REFERENCES

(1) World Alzheimer Report 2015. (2017, December 14). Retrieved from http://www.worldalzreport2015.org/.

(2) WHO | Dementia. Retrieved December 14, 2017, from http://www.who.int/mediacentre/factsheets/fs362/en/.

(3) Brookmeyer, R., Johnson, E., Ziegler-Graham, K., and Arrighi, H. M. (2007) Forecasting the global burden of Alzheimer's disease. *Alzheimer's Dementia 3* (3), 186−191.

(4) Kepp, K. P. (2012) Bioinorganic Chemistry of Alzheimer's Disease. *Chem. Rev. 112* (10), 5193−5239.

(5) Karantzoulis, S., and Galvin, J. E. (2011) Distinguishing Alzheimer's disease from other major forms of dementia. *Expert Rev. Neurother. 11* (11), 1579−1591.

(6) Kobayashi, M., Kinjo, T., Koseki, Y., Bourne, C. R., Barrow, W. W., and Aoki, S. (2014) Identification of Novel Potential Antibiotics against Staphylococcus Using Structure-Based Drug Screening Targeting Dihydrofolate Reductase. *J. Chem. Inf. Model. 54* (4), 1242−1253.

(7) Hardy, J., and Higgins, G. (1992) Alzheimer's disease: the amyloid cascade hypothesis. *Science 256* (5054), 184−185.

(8) Masters, C. L., Simms, G., Weinman, N. A., Multhaup, G., McDonald, B. L., and Beyreuther, K. (1985) Amyloid plaque core protein in Alzheimer disease and Down syndrome. *Proc. Natl. Acad. Sci. U. S. A. 82* (12), 4245−4249.

(9) Gibson, G. E., and Huang, H.-M. (2005) Oxidative stress in Alzheimer's disease. *Neurobiol. Aging 26* (5), 575−578.

(10) Honda, K., Casadesus, G., Petersen, R. B., Perry, G., and Smith, M. A. (2004) Oxidative Stress and Redox-Active Iron in Alzheimer's Disease. *Ann. N. Y. Acad. Sci. 1012* (1), 179−182.

(11) Scott, L. E., and Orvig, C. (2009) Medicinal Inorganic Chemistry Approaches to Passivation and Removal of Aberrant Metal Ions in Disease. *Chem. Rev. 109* (10), 4885−4910.

(12) Greenough, M. A., Camakaris, J., and Bush, A. I. (2013) Metal dyshomeostasis and oxidative stress in Alzheimer's disease. *Neurochem. Int. 62* (5), 540−555.

(13) Kozlowski, H., Luczkowski, M., Remelli, M., and Valensin, D. (2012) Copper, zinc and iron in neurodegenerative diseases (Alzheimer's, Parkinson's and prion diseases). *Coord. Chem. Rev. 256* (19), 2129−2141.

(14) Chakroborty, S., and Stutzmann, G. E. (2011) Early calcium dysregulation in Alzheimer's disease: setting the stage for synaptic dysfunction. *Sci. China: Life Sci. 54* (8), 752−762.

(15) Selkoe, D. J. (1991) The molecular pathology of Alzheimer's disease. *Neuron 6* (4), 487−498.

(16) Walsh, D. M., Klyubin, I., Fadeeva, J. V., Cullen, W. K., Anwyl, R., Wolfe, M. S., Rowan, M. H., and Selkoe, D. J. (2002) Naturally secreted oligomers of amyloid β protein potently inhibit hippocampal long-term potentiation in vivo. *Nature 416* (6880), 535−539.

(17) Haass, C. (1999) The Presenilins in Alzheimer's Disease−Proteolysis Holds the Key. *Science 286* (5441), 916−919.

(18) Cleary, J. P., Walsh, D. M., Hofmeister, J. J., Shankar, G. M., Kuskowski, M. A., Selkoe, D. J., and Ashe, K. H. (2005) Natural oligomers of the amyloid-protein specifically disrupt cognitive function. *Nat. Neurosci. 8* (1), 79−84.

(19) Teich, A. F., and Arancio, O. (2012) Is the Amyloid Hypothesis of Alzheimer's disease therapeutically relevant? *Biochem. J. 446* (2), 165−177.

(20) Hardy, J. (2006) Alzheimer's disease: The amyloid cascade hypothesis: An update and reappraisal. *J. Alzheimer's Dis. 9* (s3), 151−153.

(21) Hardy, J. (2002) The Amyloid Hypothesis of Alzheimer's Disease: Progress and Problems on the Road to Therapeutics. *Science 297* (5580), 353−356.

(22) Somavarapu, A. K., and Kepp, K. P. (2015) Direct Correlation of Cell Toxicity to Conformational Ensembles of Genetic Aβ Variants. *ACS Chem. Neurosci. 6* (12), 1990−1996.

(23) Kepp, K. P. (2016) Alzheimer's disease due to loss of function: A new synthesis of the available data. *Prog. Neurobiol. 143* (Suppl C), 36−60.

(24) Rauk, A. (2009) The chemistry of Alzheimer's disease. *Chem. Soc. Rev. 38* (9), 2698−2715.

DOI: 10.1021/acschemneuro.8b00210
ACS Chem. Neurosci. 2018, 9, 2795−2806

(25) Kepp, K. P. (2017) Alzheimer's disease: How metal ions define β-amyloid function. *Coord. Chem. Rev. 351*, 127−159.
(26) Warmlander, S., Tiiman, A., Abelein, A., Luo, J., Jarvet, J., Söderberg, K., Danielsson, J., and Graslund, A. (2013) Biophysical studies of the amyloid β-peptide: interactions with metal ions and small molecules. *ChemBioChem 14* (14), 1692−1704.
(27) Vivekanandan, S., Brender, J. R., Lee, S. Y., and Ramamoorthy, A. (2011) A partially folded structure of amyloid-beta(1−40) in an aqueous environment. *Biochem. Biophys. Res. Commun. 411* (2), 312−316.
(28) Sticht, H., Bayer, P., Willbold, D., Dames, S., Hilbich, C., Beyreuther, K., and Rösch, P. (1995) Structure of amyloid A4-(1−40)-peptide of Alzheimer's disease. *Eur. J. Biochem. 233* (1), 293−298.
(29) Somavarapu, A. K., and Kepp, K. P. (2015) The Dependence of Amyloid-β Dynamics on Protein Force Fields and Water Models. *ChemPhysChem 16* (15), 3278−3289.
(30) Coles, M., Bicknell, W., Watson, A. A., Fairlie, D. P., and Craik, D. J. (1998) Solution Structure of Amyloid β-Peptide(1−40) in a Water−Micelle Environment. Is the Membrane-Spanning Domain Where We Think It Is? *Biochemistry 37* (31), 11064−11077.
(31) Haass, C., and Selkoe, D. J. (2007) Soluble protein oligomers in neurodegeneration: lessons from the Alzheimer's amyloid β-peptide. *Nat. Rev. Mol. Cell Biol. 8* (2), 101.
(32) Hefti, F., Goure, W. F., Jerecic, J., Iverson, K. S., Walicke, P. A., and Krafft, G. A. (2013) The case for soluble Aβ oligomers as a drug target in Alzheimer's disease. *Trends Pharmacol. Sci. 34* (5), 261−266.
(33) Glabe, C. G. (2006) Common mechanisms of amyloid oligomer pathogenesis in degenerative disease. *Neurobiol. Aging 27* (4), 570−575.
(34) Hung, L. W., Ciccotosto, G. D., Giannakis, E., Tew, D. J., Perez, K., Masters, C. L., and Barnham, K. J. (2008) Amyloid-β Peptide (Aβ) Neurotoxicity Is Modulated by the Rate of Peptide Aggregation: Aβ Dimers and Trimers Correlate with Neurotoxicity. *J. Neurosci. 28* (46), 11950−11958.
(35) Lovell, M. A. (2009) A Potential Role for Alterations of Zinc and Zinc Transport Proteins in the Progression of Alzheimer's Disease. *J. Alzheimer's Dis. 16* (3), 471−483.
(36) Shcherbatykh, I., and Carpenter, D. O. (2007) The role of metals in the etiology of Alzheimer's disease. *J. Alzheimer's Dis. 11* (2), 191−205.
(37) Maynard, C. J., Bush, A. I., Masters, C. L., Cappai, R., and Li, Q.-X. (2005) Metals and amyloid-β in Alzheimer's disease. *Int. J. Exp. Pathol. 86* (3), 147−159.
(38) Bush, A. I. (2003) The metallobiology of Alzheimer's disease. *Trends Neurosci. 26* (4), 207−214.
(39) Barnham, K. J., Masters, C. L., and Bush, A. I. (2004) Neurodegenerative diseases and oxidative stress. *Nat. Rev. Drug Discovery 3* (3), 205−214.
(40) Smith, D. P., Ciccotosto, G. D., Tew, D. J., Fodero-Tavoletti, M. T., Johanssen, T., Masters, C. L., and Cappai, R. (2007) Concentration Dependent Cu2+ Induced Aggregation and Dityrosine Formation of the Alzheimer's Disease Amyloid-β Peptide. *Biochemistry 46* (10), 2881−2891.
(41) Huang, X., Cuajungco, M. P., Atwood, C. S., Hartshorn, M. A., Tyndall, J. D., Hanson, G. R., and Bush, A. I. (1999) Cu(II) potentiation of alzheimer abeta neurotoxicity. Correlation with cell-free hydrogen peroxide production and metal reduction. *J. Biol. Chem. 274* (52), 37111−6.
(42) Jomova, K., Vondrakova, D., Lawson, M., and Valko, M. (2010) Metals, oxidative stress and neurodegenerative disorders. *Mol. Cell. Biochem. 345* (1−2), 91−104.
(43) Dorlet, P., Gambarelli, S., Faller, P., and Hureau, C. (2009) Pulse EPR spectroscopy reveals the coordination sphere of copper(II) Ions in the 1−16 amyloid-β peptide: A key role of the first two N-terminus residues. *Angew. Chem., Int. Ed. 48* (49), 9273−9276.
(44) Drew, S. C., Masters, C. L., and Barnham, K. J. (2009) Alanine-2 Carbonyl is an Oxygen Ligand in Cu 2+ Coordination of Alzheimer's Disease Amyloid-β Peptide − Relevance to N-Terminally Truncated Forms. *J. Am. Chem. Soc. 131* (25), 8760−8761.
(45) Streltsov, V. A., Titmuss, S. J., Epa, V. C., Barnham, K. J., Masters, C. L., and Varghese, J. N. (2008) The Structure of the Amyloid-β Peptide High-Affinity Copper II Binding Site in Alzheimer Disease. *Biophys. J. 95* (7), 3447−3456.
(46) Minicozzi, V., Stellato, F., Comai, M., Dalla Serra, M., Potrich, C., Meyer-Klaucke, W., and Morante, S. (2008) Identifying the minimal copper- and zinc-binding site sequence in amyloid-beta peptides. *J. Biol. Chem. 283* (16), 10784−92.
(47) Drew, S. C., and Barnham, K. J. (2011) The heterogeneous nature of Cu2+ interactions with Alzheimer's amyloid-β peptide. *Acc. Chem. Res. 44* (11), 1146−1155.
(48) Barnham, K. J., Kenche, V. B., Ciccotosto, G. D., Smith, D. P., Tew, D. J., Liu, X., Cappai, R., et al. (2008) Platinum-based inhibitors of amyloid- as therapeutic agents for Alzheimer's disease. *Proc. Natl. Acad. Sci. U. S. A. 105* (19), 6813−6818.
(49) Man, B. Y.-W., Chan, H.-M., Leung, C.-H., Chan, D. S.-H., Bai, L.-P., Jiang, Z.-H., and Ma, D.-L. (2011) Group 9 metal-based inhibitors of β-amyloid (1−40) fibrillation as potential therapeutic agents for Alzheimer's disease. *Chemical Science 2* (5), 917−921.
(50) Ma, G., Wang, E., Wei, H., Wei, K., Zhu, P., and Liu, Y. (2013) PtCl2(phen) disrupts the metal ions binding to amyloid-β peptide. *Metallomics 5* (7), 879.
(51) Streltsov, V. A., Epa, V. C., James, S. A., Churches, Q. I., Caine, J. M., Kenche, V. B., and Barnham, K. J. (2013) Structural insights into the interaction of platinum-based inhibitors with the Alzheimer's disease amyloid-beta peptide. *Chem. Commun. 49* (97), 11364−11366.
(52) Furlan, S., Hureau, C., Faller, P., and La Penna, G. (2010) Modeling the Cu + Binding in the 1−16 Region of the Amyloid-β Peptide Involved in Alzheimer's Disease. *J. Phys. Chem. B 114* (46), 15119−15133.
(53) La Penna, G., Hureau, C., Andreussi, O., and Faller, P. (2013) Identifying, By First-Principles Simulations, Cu[Amyloid-β] Species Making Fenton-Type Reactions in Alzheimer's Disease. *J. Phys. Chem. B 117* (51), 16455−16467.
(54) Alí-Torres, J., Maréchal, J.-D., Rodríguez-Santiago, L., and Sodupe, M. (2011) Three Dimensional Models of Cu2+-Aβ(1−16) Complexes from Computational Approaches. *J. Am. Chem. Soc. 133* (38), 15008−15014.
(55) Alí-Torres, J., Mirats, A., Maréchal, J.-D., Rodríguez-Santiago, L., and Sodupe, M. (2015) Modeling Cu^{2+}-Aβ complexes from computational approaches. *AIP Adv. 5* (9), 092402.
(56) Raffa, D. F., and Rauk, A. (2007) Molecular Dynamics Study of the Beta Amyloid Peptide of Alzheimer's Disease and Its Divalent Copper Complexes. *J. Phys. Chem. B 111* (14), 3789−3799.
(57) Huy, P. D. Q., Vuong, Q. V., La Penna, G., Faller, P., and Li, M. S. (2016) Impact of Cu(II) Binding on Structures and Dynamics of Aβ42 Monomer and Dimer: Molecular Dynamics Study. *ACS Chem. Neurosci. 7* (10), 1348−1363.
(58) Burton, V. J., Deeth, R. J., Kemp, C. M., and Gilbert, P. J. (1995) Molecular Mechanics for Coordination-Complexes - the Impact of Adding D-Electron Stabilization Energies. *J. Am. Chem. Soc. 117* (32), 8407−8415.
(59) Burton, V. J., and Deeth, R. J. (1995) Molecular modelling for copper(II) centres. *J. Chem. Soc., Chem. Commun. 5*, 573−574.
(60) Deeth, R. J., Fey, N., and Williams-Hubbard, B. (2005) DommiMOE: An implementation of ligand field molecular mechanics in the molecular operating environment. *J. Comput. Chem. 26* (2), 123−130.
(61) Deeth, R. J., Anastasi, A., Diedrich, C., and Randell, K. (2009) Molecular modelling for transition metal complexes: Dealing with d-electron effects. *Coord. Chem. Rev. 253* (5−6), 795−816.
(62) Deeth, R. J., and Hearnshaw, L. J. A. (2006) Molecular modelling of Jahn−Teller distortions in Cu(II)N6 complexes: elongations, compressions and the pathways in between. *Dalton Trans. 8*, 1092−1100.
(63) Deeth, R. J., and Randell, K. (2008) Ligand Field Stabilization and Activation Energies Revisited: Molecular Modeling of the

DOI: 10.1021/acschemneuro.8b00210
ACS Chem. Neurosci. 2018, 9, 2795−2806

Thermodynamic and Kinetic Properties of Divalent, First-Row Aqua Complexes. *Inorg. Chem. 47* (16), 7377−7388.
(64) Anastasi, A. E., and Deeth, R. J. (2009) Capturing the Trans Influence in Low-Spin d(8) Square-Planar Platinum(II) Systems using Molecular Mechanics. *J. Chem. Theory Comput. 5* (9), 2339−2352.
(65) Tai, H.-C., Brodbeck, R., Kasparkova, J., Farrer, N. J., Brabec, V., Sadler, P. J., and Deeth, R. J. (2012) Combined Theoretical and Computational Study of Interstrand DNA Guanine−Guanine Cross-Linking by trans -[Pt(pyridine) 2] Derived from the Photoactivated Prodrug trans,trans,trans -[Pt(N 3) 2 (OH) 2 (pyridine) 2]. *Inorg. Chem. 51* (12), 6830−6841.
(66) Mutter, S. T., Deeth, R. J., Turner, M., and Platts, J. A. (2018) Benchmarking of copper(II) LFMM parameters for studying amyloid-β peptides. *J. Biomol. Struct. Dyn. 36* (5), 1145−1153.
(67) Turner, M., Platts, J. A., and Deeth, R. J. (2016) Modeling of Platinum-Aryl Interaction with Amyloid-β Peptide. *J. Chem. Theory Comput. 12* (3), 1385−1392.
(68) Turner, M., Deeth, R. J., and Platts, J. A. (2017) Prediction of ligand effects in platinum-amyloid-β coordination. *J. Inorg. Biochem. 173*, 44−51.
(69) Turner, M., Mutter, S. T., Deeth, R. J., and Platts, J. A. (2018) Ligand field molecular dynamics simulation of Pt(II)-phenanthroline binding to N-terminal fragment of amyloid-β peptide. *PLoS One 13* (3), e0193668.
(70) Baumketner, A., Bernstein, S. L., Wyttenbach, T., Bitan, G., Teplow, D. B., Bowers, M. T., and Shea, J.-E. (2006) Amyloid beta-Protein Monomer Structure: A Computational and Experimental Study. *Protein Sci. 15* (3), 420−428.
(71) Yang, M., and Teplow, D. B. (2008) Amyloid beta-Protein Monomer Folding: Free-Energy Surfaces Reveal Alloform-Specific Differences. *J. Mol. Biol. 384* (2), 450−464.
(72) Sciarretta, K. L., Gordon, D. J., Petkova, A. T., Tycko, R., and Meredith, S. C. (2005) Aβ40-lactam(D23/K28) models a conformation highly favorable for nucleation of amyloid. *Biochemistry 44* (16), 6003−6014.
(73) Smith, W., Yong, C. W., and Rodger, P. M. (2002) DL_POLY: Application to molecular simulation. *Mol. Simul. 28* (5), 385−471.
(74) Cornell, W. D., Cieplak, P., Bayly, C. I., Gould, I. R., Merz, K. M., Ferguson, D. M., Spellmeyer, D. C., Fox, T., Caldwell, J. W., and Kollman, P. A. (1995) A Second Generation Force Field for the Simulation of Proteins, Nucleic Acids, and Organic Molecules. *J. Am. Chem. Soc. 117*, 5179−5197.
(75) Molecular Operating Environment (MOE) (2013). 1010 Sherbooke St. West, Suite #910, Chemical Computing Group Inc., Montreal, QC, Canada, H3A 2R7.
(76) Labute, P. (2010) LowModeMD—Implicit Low-Mode Velocity Filtering Applied to Conformational Search of Macrocycles and Protein Loops. *J. Chem. Inf. Model. 50* (5), 792−800.
(77) Yong, C. W. (2016) Descriptions and Implementations of DL_F Notation: A Natural Chemical Expression System of Atom Types for Molecular Simulations. *J. Chem. Inf. Model. 56* (8), 1405−1409.
(78) Ryckaert, J.-P., Ciccotti, G., and Berendsen, H. J. C. (1977) Numerical integration of the cartesian equations of motion of a system with constraints: molecular dynamics of n-alkanes. *J. Comput. Phys. 23* (3), 327−341.
(79) Humphrey, W., Dalke, A., and Schulten, K. (1996) VMD: visual molecular dynamics. *J. Mol. Graphics 14* (1), 33−38.
(80) Frishman, D., and Argos, P. (1995) Knowledge-based protein secondary structure assignment. *Proteins: Struct., Funct., Genet. 23* (4), 566−579.
(81) Gracia, L. (2014) *iTrajComp plugin for VMD*. Retrieved April 26, 2018, from http://physiology.med.cornell.edu/faculty/hweinstein/vmdplugins/itrajcomp/.

DOI: 10.1021/acschemneuro.8b00210
ACS Chem. Neurosci. 2018, 9, 2795−2806